Direct Inlet Probe Atmospheric Pressure Photo and Chemical Ionization Coupled to Ultrahigh Resolution Mass Spectrometry for the Description of Lignocellulosic Biomass

Clément Castilla, Christopher Rüger, Stéphane Marcotte, Hélène Lavanant, Carlos Afonso

Direct inlet probe atmospheric pressure photo and chemical ionization coupled to ultra-high resolution mass spectrometry for the description of lignocellulosic biomass

Clément Castilla[1], Christopher P. Rüger[1,2], Stéphane Marcotte[1], Hélène Lavanant[1]*, Carlos Afonso[1]

1. Normandie Univ, UNIROUEN, INSA Rouen, CNRS, COBRA, 76000 Rouen, France
2. Universität Rostock, Institut für Chemie, Abteilung für Analytische und Technische Chemie, Dr.-Lorenz.-Weg 1, Rostock, DE 18059

*Corresponding Author

E-mail : helene.lavanant@univ-rouen.fr

Abstract

Lignocellulosic biomass, in particular wood, is a complex mixture containing cellulose, hemicellulose, lignin, and other trace compounds. Chemical analysis of these biomasses, especially lignin components, is a challenge. Lignin is a highly reticulated polymer that is poorly soluble and usually requires chemical, enzymatic, or thermal degradation for its analysis. Here, we studied the thermal degradation of lignocellulosic biomass using a direct insertion probe (DIP). DIP was used with two ionization sources: atmospheric pressure chemical ionization (APCI) and atmospheric pressure photoionization (APPI) coupled to ultra-high-resolution mass spectrometry. Beech lignocellulosic biomass sample were used to develop the DIP-APCI/APPI methodology. Two other wood species (maple and oak) were analyzed after optimization of DIP parameters. The two ionization sources were compared at first and showed different response towards beech sample, according to the source specificity. APPI was more specific to lignin degradation compounds, whereas APCI covered a larger variety of oxygenated compounds, *e.g.*, fatty acids, polyphenolics compounds, in addition to lignin degradation products. The study of the thermo-desorption profile gave information on the different steps of lignocellulosic biomass pyrolysis. The comparison of the three feed sample types (oak, maple, and beech), using principal component analysis (PCA) with DIP-APCI experiments, showed molecular level differences between beech wood pellets and the two others wood species (maple and oak).

Keywords*:* direct inlet probe, high-resolution mass spectrometry, biomass, APPI, APCI

Introduction

Lignocellulosic biomass, such as wood, is an abundant and renewable source of energy that can be used as an alternative to fossil fuel, *e.g.*, directly for heating purposes or after conversion as biofuel. In recent years household heating with wood pellets has become more and more popular, related to traditional logwood stove heating. Furthermore, bio-oils obtained by pyrolysis of lignocellulosic biomass are already generated in various plants on an industrial scale.[1] Thus, the overall use of lignocellulosic biomass has been drastically increasing, resulting in an intensified need to investigate the evolution of the molecular composition during the combustion and pyrolysis process. This knowledge will be beneficial for the optimization of biofuel generation. The latter is particularly critical regarding environmental health and climate change.[2,3]

Lignocellulosic biomass is a complex mixture containing cellulose, hemicellulose, lignin, and other trace compounds. Lignin is a highly reticulated bio-polymer that is poorly soluble and usually requires chemical,[4] fungal,[5,6] or thermal degradation for analysis.[7]

Evolved gas analysis (EGA) is one approach to tackle the molecular complexity focusing on the volatile and semi-volatile compounds, as well as pyrolysis products of the solid lignocellulosic biomass feed. More specifically, thermogravimetry (TG) and differential scanning calorimetry (DSC) coupled to a suitable analytical system, can give information on the chemical decomposition of the sample.[8] In this respect, the coupling with mass spectrometry (MS) presents a rich potential to identify and quantify the evolved gas mixture[9-10]. Moreover, the additional implementation of a gas chromatographic (GC) separation step or a fast pyrolysis injector GC system can provide further structural information.

Direct insertion probe (DIP) is a rapid and simple technique, well suited for solid samples. The sample is placed in an inert support and heated to a controlled temperature. In contrast to most EGA techniques, the sample is volatilized directly in the ionization source of the mass spectrometer. Thus, released gaseous components are directly ionized and subsequently analyzed by the MS. As a significant benefit, DIP allows the analysis of solids with no sample preparation, which can be advantageous for the insoluble solid biomass feed.

The direct insertion probe can be coupled to vacuum or atmospheric pressure ionization sources. The most commonly used vacuum ionization source with DIP is electron ionization (EI). EI has been used with different samples, *e.g.,* polymers,[11] crude oil,[12] bitumen,[13] asphaltenes,[14] or biomass.[15] However, EI leads to a high rate of fragmentation of molecules, making mass spectra more complex and challenging to interpret. Hence, with the development of atmospheric pressure sources such as chemical ionization (APCI) and photo ionization (APPI), direct analysis devices were developed, such as atmospheric pressure solids analysis probe (ASAP)[16] or DIP-APCI/APPI. These probes can handle solid samples using pyrolysis by a heated nitrogen gas stream near the ionization region. The analysis time is short, and the soft ionization grants minimal fragmentation of ions compared to electron ionization. Various studies used the ASAP source, *e.g.*, for petroleum samples,[17] polymers,[18] and aerosols.[19] For the analysis of a complex mixture such as lignin pyrolysis products, the use of ultra-high resolution mass resolving power is recommended. As a matter of fact, the common mass differences for $C_cH_hN_nO_o$ compounds are: 36.4 mDa (O and CH_4), 8.9 mDa ($^{13}C_2$ and H_2) and 8.2 mDa (N and ^{13}CH).[20] These mass differences require the use of an ultra-high-resolution mass spectrometer (R≥200,000). In this respect, Fourier transform ion cyclotron resonance mass spectrometry (FTICR MS) with its unbeaten resolving power and mass accuracy, is able to resolve isobaric compounds and give in-depth information on the molecular composition. Numerous applications were shown deploying FTICR MS for the analysis of highly complex mixtures, such as petroleum,[21] aerosols[22] or polymers.[23] Most often these works were performed using direct infusion techniques of soluble or extracted sample material.

In this study, we aimed to develop a versatile, fast, and robust methodology for the molecular description of biomass combustion feed materials with various pellet types and minimal sample preparation. For this purpose, a direct inlet probe with atmospheric pressure ionization sources hyphenated to FTICR mass spectrometry was used, which allows a comprehensive analysis of the evolved gas mixture.

Beech pellets, whose pyrolysis compounds are well described in literature,[24] were used to compare APPI and APCI sources in the positive ion mode. Although APPI is commonly used for complex matrix analyses by direct infusion, including several studies of bio-oils generated by biomass pyrolysis, only a few APPI mass spectrometric studies focus on the pyrolysis process.[25] APCI was chosen due to its capacity to ionize oxygenated species commonly abundant in biomass pyrolysis and combustion products.[26] Here, we monitored the pyrolysis process in evolved gas analysis. Finally, we compared three different individual pellet types, beech, oaf, and maple, to address the molecular differences and similarities in lignocellulose biomass.

Method and Material

Sample material

For this study, three different wood pellet types were studied: beech (Ooni), oak, and maple (Traeger Pellet Grills). The wood pellet was ground for two minutes, using an A 10 basic mill (IKA Mills) with a water cooling system at approximately 15°C (Figure S1).

Instrumentation

Mass spectra were acquired using a 12 T ultra-high resolution Fourier transform ion cyclotron resonance mass spectrometer (SolariX XR FTMS, Bruker Daltonics). The sample introduction was performed by utilizing the DirectProbe DIP (Bruker) that can be introduced into the APCI and APPI source (Figure S2). Approximately (0.4 ± 0.1) mg of sample material was trapped into the capillary tube by using a small piece of clean quartz fiber filters (Figure S3) then directly introduced into the ionization source after acquisition start. The start of the thermo-desorption and pyrolysis process was prompted by a heated gas stream. The presence of the quartz filter in the glass capillary tube induced a delay of evaporation of the sample. Such delay was found beneficial to avoid high ion currents during the thermo-desorption process and thus ensure regular ion transmission and acquisition. Each sample was analyzed in four replicates.

For ionization, an APCI and an APPI source were used. Source parameters were chosen to ensure a robust, sensitive, and reproducible analysis of the biomass samples. These parameters were set the same for the two sources to be comparable. The nitrogen nebulizer gas was set at a pressure of 3 bar and 400°C and a nitrogen drying gas flow of 2 L/min at 200°C. The corona current from APCI source was set to 3 µA (Table S1 for source and acquisition parameters). The chosen mass range for this study was *m/z* 122.8 to *m/z* 1,000 as low mass degradation products are well described in GC-MS studies.[27] Moreover, Fourier transform ion cyclotron resonance mass spectrometer performs better in this mass range. The analog image current was digitized with 2 million data points resulting in the recording of a 0.7 s time-domain signal, which was transformed into the corresponding frequency domain by Fourier transform (one zero-fill and full-sine apodization). As resolving power scales with transient length, this 0.7s transient allowed a compromise between the scan frequency of the thermo-desorption profile (< 3 min) and the resolving power required to differentiate the common isobaric $C_cH_hN_nO_o$ compounds.[20] A resolution of 400,000 was obtained at *m/z* 200.

Data analysis

External calibration of mass spectra were performed using a polycyclic aromatic hydrocarbon (PAH) standard mixture (Supelco EPA 610, Sigma Aldrich) containing 16 different PAH and measured with the same instrumental conditions. Internal calibration was performed on an average spectrum generated over the complete analysis using different series of oxygenated compounds. Generally, for linear correction, a standard deviation below 250 ppb was found. After calibration, each individual scan of the time-resolved data was peak picked (S/N 9) and exported with Bruker Data Analysis (5.0) visual basic scripts. The exported mass spectra were processed by self-written MATLAB routines, and molecular assignation was performed using the following restrictions: $C_cH_hN_nO_o$; n≤1 and o≤10, with a maximum error of 2 ppm, DBE≤80, 0 ≤ H/C ratio ≤ 3. The maximum number of oxygen atoms of ten was chosen after trying different boundaries (o≤10, o≤15 and o≤20) and determining the best ratio between number of attribution and the attribution errors. The molecular classes with more than ten oxygen atoms represented less than 0.04% of the relative summed intensity (for o≤20). The final assignment lists were further treated with MATLAB to create an average assignation list common to at least three replicates (out of four). Visualization of the data was done using OriginPro (2016) and Matlab R2018b.

For maple, beech, and oak samples and each replicate measurements, the elemental composition attributions of average spectra were compared via multivariate data analysis. These replicate measurements were randomized. All attributions are considered, and attributions not found within a sample are set to zero intensity. The known group structure (replicates of a sample type, supervised statistics) was included in the analysis by applying analysis of variance (ANOVA). Features with p-values below 0.01 were regarded as statistically significant and selected as input variables for the Principal Component Analysis (PCA). This procedure was done to reduce the number of variables (elemental compositions). For this purpose, the data (abundance) needed to be normalized. Here, power transformation and variable stability scaling (VAST) were performed. This procedure ensures that low-abundant signals can be efficiently identified as potential marker species in the statistics. Thus, the importance for the PCA is not linked to the raw abundance but to the variance and differences of the replicate means. Consecutively, PCA was performed on those pre-processed data. The resulting scores and loadings data, in combination with the elemental composition attribution, were used for visualization. In this respect, score data are linked to the experiments (replicates and sample type) and loadings data to the individual elemental compositions (molecular profile).

Results and Discussion

Source parameters optimization and DIP-APCI/APPI comparison

DIP-APCI and DIP-APPI sources were firstly compared using ground pellet samples. The sample was quickly inserted to observe the fast pyrolysis process of the pellet, which should primarily lead to low mass compounds. The total ion current (TIC) resulting from the thermo-desorption profile from the pyrolysis of wood beech pellet (Figure 1), exhibited a response time of less than one minute for APPI, with fast signal decay after 30 s. In comparison, the response time for APCI was three minutes. The inset in Figure 1 represented the summed abundance for APPI and APCI with error bars as standard deviation (±1σ) from four replicates. APCI resulted in a summed abundance considerably seven times larger than APPI. APPI is sometimes used with a dopant such as toluene [28], added in the source to enhance the ionization yield. Here no dopant was used to keep experimental conditions comparable between the two sources. The absence of dopant may explain the lower total ion count of APPI compared to APCI.

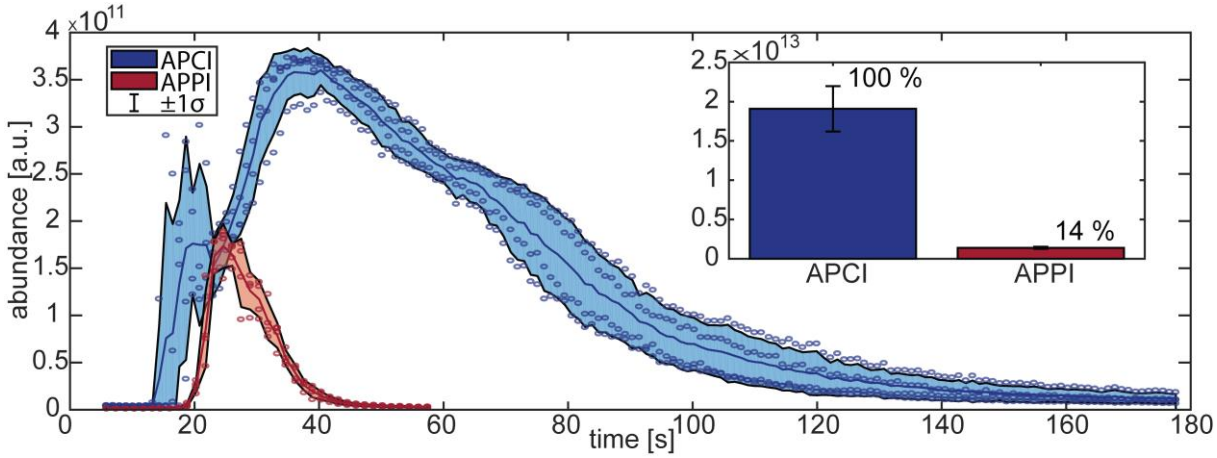

Figure 1. Time-resolved total ion count (TIC) for the DIP experiment conducted with APCI (blue) and APPI (red) on ground beech pellets. The shaded area corresponds to ±1σ, and the scattered circles are derived from individual mass spectra. The averaged summed TIC with the respective standard deviation is given in the inset.

The standard deviation given in the shaded area pointed out the reproducibility of the total ion count response with a deviation of typically below 10 %. The variation observed within the DIP-APCI profile was mainly due to variation in sample amount in the capillary. Indeed, a small 0.1 mg variation in the sample amount can induce significant changes in the desorption profile. Variation in the sample heating due to differences in the placement of the sample inside the glass capillary or the speed of sample introduction, may also cause some variation on the thermo-desorption profile.

The averaged mass spectra (Figure 2) showed a bi-modal ion distribution for both the ionization sources. The first distribution was centered around *m/z* 200, which corresponded to the expected *m/z* of lignin monomers degradation products. The apex of the second distribution was around *m/z* 350, which corresponded to the expected *m/z* of lignin dimer degradation products. These two distributions were observed with the two sources, even though the DIP-APCI spectra (Figure 2a) was more complex with a higher number of peaks as exemplarily shown in the inset in Figure 2 (enlargement of *m/z* 371).

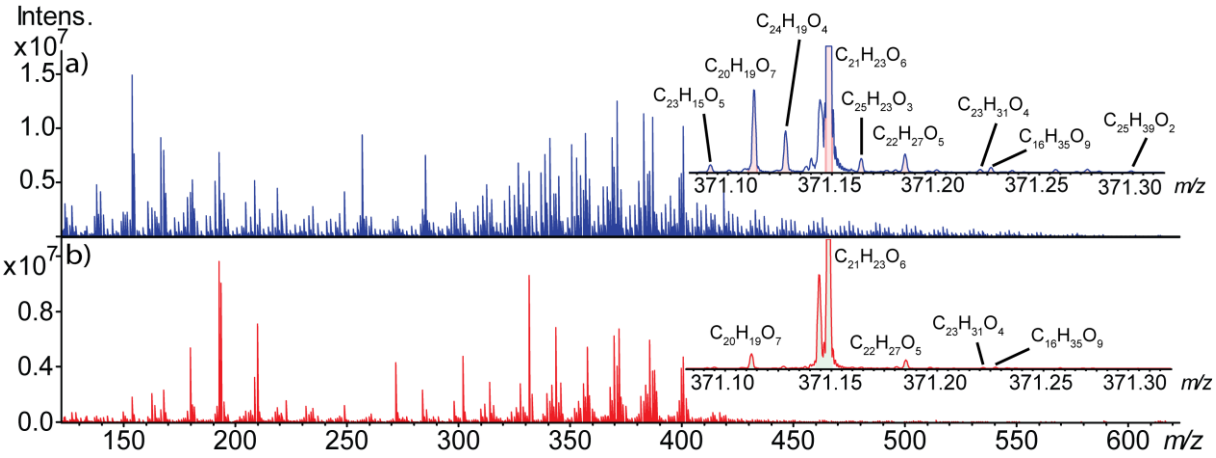

Figure 2. Average mass spectra for the DIP experiment conducted with APCI (a), and APPI (b). A zoom at a nominal mass of 371 for the two sources is shown for the two spectra.

During the pyrolysis process, small shifts of the *m/z* values were observed for most peaks due to the change of ion abundance transmitted to the ICR cell (space charge effect). These *m/z* shifts lowered the overall mass accuracy, which is critical for the accurate determination of molecular compositions (Figure S4). Thus, an additional data processing step was carried out to correct these shifts. Hence, an *m/z*-recalibration of each individual mass spectra was done to ensure a reliable molecular attribution across the entire thermo-desorption profile. For this purpose, the mass spectra, pre-calibrated using Bruker Data Analysis, were exported and re-calibrated using lab-written MATLAB scripts. These scripts applied a linear correction to each mass spectrum, using a set of well-identified ions from the samples (Table S2). Briefly, each spectrum was searched for the occurrence of the recalibration signals within a broader acceptance range of 5 ppm. If a sufficient number of signals were found, a new linear recalibration function was calculated and deployed. This procedure was performed for each scan separately. Therefore, molecular attributions errors were significantly decreased for the average mass spectra from a mean error of 0.60 ppm and a standard deviation of 0.45 ppm to a mean error of 0.33 ppm and a standard deviation of 0.34 ppm (Figure S5).

The Venn diagram [29] of the four replicates for APCI and APPI were shown in Figure S6. Roughly 4,700 different molecular attributions were found for DIP-APCI and 85% were common to the four

replicates. With DIP-APPI, 1,700 molecular attributions were found, which was less than DIP-APCI by a factor of three. Moreover, DIP-APPI was less reproducible (80% in common with the four replicates). The attribution lists of the replicates were combined as one and attributions common to three out of the four replicates were further used for graphical representation.

Figure 3 showed the attributions sorted by molecular classes depending on the number of oxygen atoms in the molecular formulae with their relative intensity and their mean DBE for the two ionization sources.

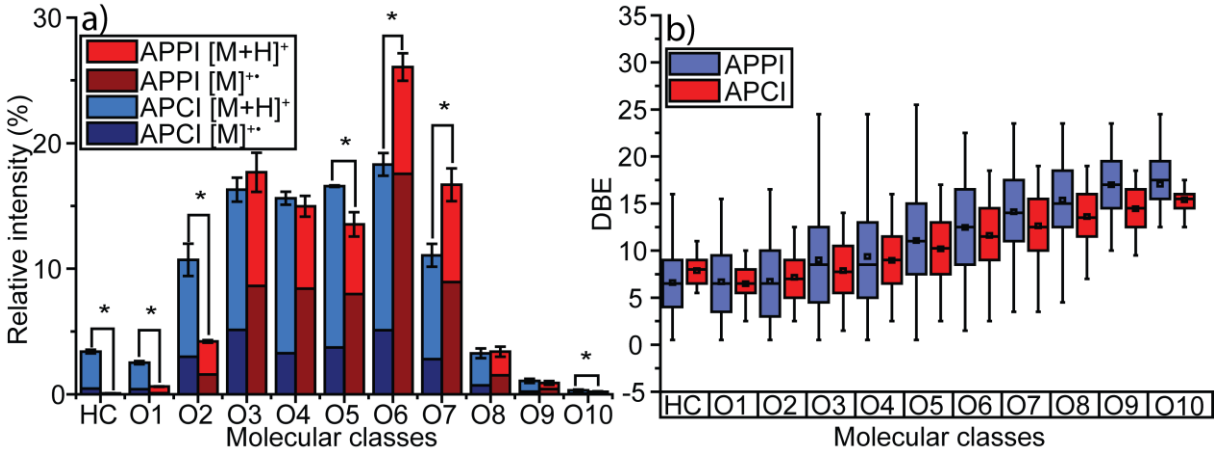

Figure 3. (a) Grouped stack histogram of the relative intensity sorted by molecular classes, depending on oxygen atom content for the DIP experiment with APCI (blue) and APPI (red). $[M+H]^+$ and $[M]^{+\bullet}$ ions proportion are shown, and error bars represent the standard deviation (*n*=4). * The asterisks signal a -significant difference as established *via* a Student t-test. (**b)** box chart corresponding to the DBE percentile values sorted by molecular classes, depending on oxygen atom content for the DIP experiment with APCI (blue) and APPI (red).

Similar to results from literature for lignocellulosic biomass or the respectively derived biofuel,[30,31] the molecular attributions were dominated by oxygenated species with two to seven oxygen atoms for the two ionization sources (89 and 93 % of TIC, respectively). However, differences between DIP-APCI and DIP-APPI could be found, especially for C_cH_h, C_cH_hO, $C_cH_hO_2$, $C_cH_hO_5$, $C_cH_hO_6$, and $C_cH_hO_7$ classes (Figure 3-a). As shown in Figure 3-a, the DIP-APPI source generated more radical cations compared to the DIP-APCI source, which generated more protonated cations. In both cases, the formation of radical species was expected under dry conditions, but the presence of water in the pellets and source atmosphere can generate protonated molecules as well.[32,33,34] Figure 3-b) shows the 5th, 25th 75th, 95th percentile, and median value of DBE for each molecular class and ionization source. The median values were higher for the APCI source and the dispersion was also higher. Conversely, the APPI DBE median values were lower with lower dispersion. The CHO_2-class was dominated by less unsaturated (low DBE) species with DIP-APCI. Conversely, CHO_6 and CHO_7 class compounds, identified as unsaturated and aromatic molecules, were found to be more abundant in DIP-APPI.

Van Krevelen[35] and mass defect *vs.* nominal mass diagrams (Figure 4) provided further information on the different molecular families observed during the pyrolysis of the beech pellets.

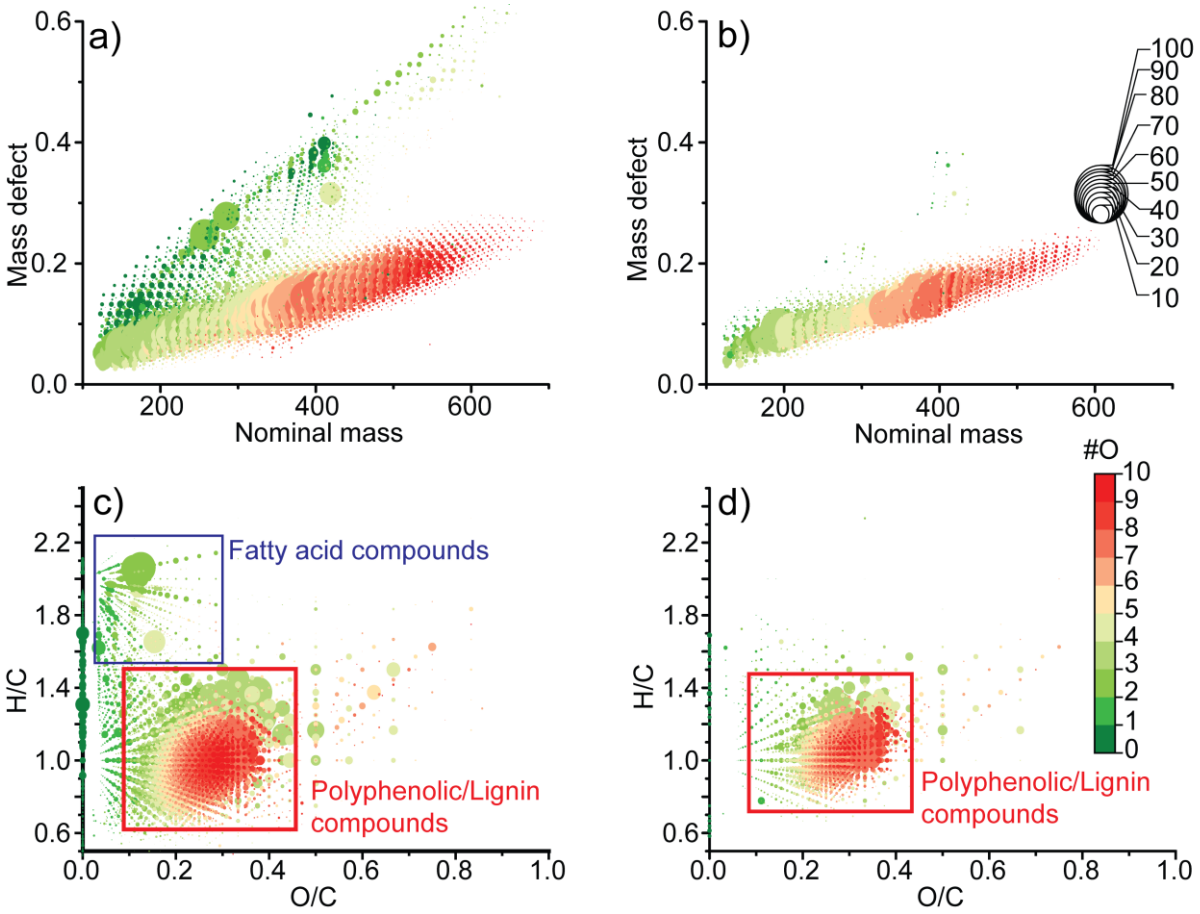

Figure 4. Molecular description plots for the DIP-experiment. Nominal mass vs. mass defect with oxygen number color-coded and relative intensity coded as dot-size: a) DIP-APCI and b) DIP-APPI. O/C Van Krevelen diagram with oxygen number color-coded and relative intensity coded as dot-size: c) DIP-APCI and d) DIP-APPI.

Nominal mass *vs.* mass defect plots (Figures 4a and 4b) are giving information on the chemical space of molecular attribution for $C_cH_hN_{0-1}O_{0-10}$ classes by using their mass defect and oxygen number (represented by color). For APCI, two distributions were observed: one with mass defect up to 0.6 and low oxygen number, and a second distribution with a mass defect up to 0.2 and zero to ten oxygen. Compounds with a high mass defect were not observed in DIP-APPI. The Van Krevelen plots (Figures 4c and 4d) provided similar information using the O/C and H/C molecular ratio of attributed formulas. Two main distributions were found with APCI. The first one included H/C ratios between 1.5 and 2.4, as well as O/C between 0.1 and 0.2 with a low number of oxygen. The other distribution with H/C ratios between 0.5 and 1.5, O/C between 0.1 and 0.5 containing zero to ten oxygen. Only the second distribution with H/C ratios between 0.5 and 1.5, O/C between 0.1 and 0.5 containing zero to ten oxygen was observed in DIP-APPI. The compounds with low mass defect could be associated with low H/C ratio, because of the mass of hydrogen (m(H) = 1.0078 u). High O/C ratio could also lead to low mass defect as oxygen have a negative mass defect (m(O) = 15.9949 u), but here, the bulk of the compounds contained three to seven oxygen resulting in low O/C ratio. So, low H/C ratio was the dominant factor affecting mass defect. Formulae with low mass defect and H/ C ratios were consistent with aromatic compounds such as polyphenolic compounds deriving from the degradation of lignin. These lignin degradation products were observed in both DIP-APCI and DIP-APPI mass spectra. In contrast, the compounds with high mass defects, associated with a high H/C ratio, and low oxygen

atoms numbers were consistent with aliphatic compounds, e.g., fatty acids or lipids. Such compounds were only observed in DIP-APCI. However, the cellulose region in the Van Krevelen diagram with 0.8 <O/C< 1 and 1.5 <H/C< 2, was empty for the two ionization sources. The absence of cellulose could be attributed to the high nebulizer gas temperature of 400°C, which most likely caused significant depolymerization of cellulose. The degradation was expected to be extensive, thus causing the conversion of cellulose-like compounds yielding mostly levoglucosan, 5-hydroxymethylfurfural and flammable volatile.[36,37,38]

Expectedly the hydrocarbon molecular class was observed only with APCI. Indeed, the APCI source produces a nitrogen plasma in which ionization will involve charge exchange processes between molecules and ionized nitrogen.[39] As nitrogen has an ionization energy of 15 eV, it is more energetic than APPI photons. As a consequence, APCI can ionize more efficiently low DBE species such as fatty acids or saturated hydrocarbon. That explains the differences between the two sources for hydrocarbon class compounds.

APPI was therefore found to be more specific to lignin degradation products with high aromaticity, APCI could be regarded as a more general source, covering a larger variety of oxygenated compounds(*e.g.*, fatty acids, polyphenolics compounds), in addition to lignin degradation products. Hence, DIP-APCI was chosen as an ionization source for further analysis within this study.

Thermo-desorption and pyrolysis profile

After choosing DIP-APCI as the more comprehensive ionization source for the non-targeted analysis of lignocellulosic biomass pyrolysis products, four different regions of the thermo-desorption/pyrolysis profile were studied (Figure 5). The thermo-desorption and pyrolysis was done with isothermal parameters (nebulizer gas at 400°C and drying gas at 200°C).

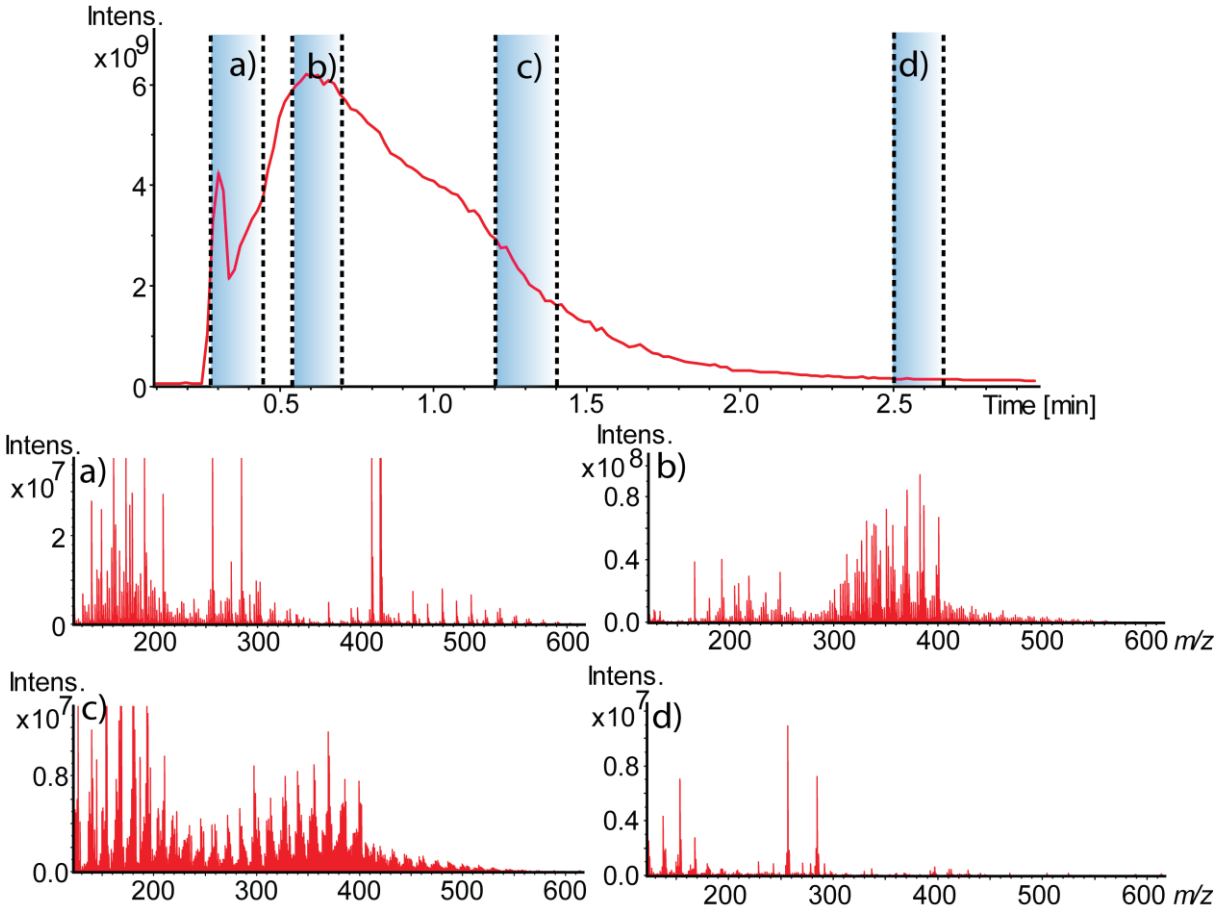

Figure 5. Thermo-desorption profile of beech pellet samples. Mass spectra were extracted from several regions of the profile with a), start of thermo-desorption, b), transition to pyrolysis products c), main pyrolysis phase and d), residual release.

An average mass spectrum was extracted for four selected time scans (named a, b, c, and d) to monitor the pyrolysis process. The mass spectrum in Figure 5a, averaged from 0.28 min to 0.41 min, is corresponding to the start of the desorption profile. It expectedly contained the most volatile compounds from wood and the volatile species which were adsorbed on the quartz fiber filters. The mass spectrum averaged from 0.52 min to 0.7 min, (Figure 5b), corresponded to the maximum abundance of ions, and was the transition to main pyrolysis products. Here, two ion distributions were observed, one peaking at roughly *m/z 200* and another one, the most abundant, with an apex at *m/z 350*. In the mass spectrum averaged from 1.24 min to 1.40 min (Figure 5c), when the ion abundance decreased, the same bi-modal distribution was observed. The two ions distributions had equivalent intensities. The mass spectrum averaged from 2.50 min to 2.67 min (Figure 5d), corresponding to the last ions observed in the pyrolysis process, was mainly composed of low mass signals. Attribution lists were obtained from the average mass spectrum of the four regions. Attribution lists of the four analytical replicates were compared using Venn diagrams (Figure S7). Around 80% of attribution were common to four replicates for all the selected regions except for the last one, with 70% of common attribution. The molecular attributions were represented, in different graphical representations, to visualize molecular information throughout the four selected time section of the thermo-desorption profile (Figure 6). The first histogram described the relative intensities of attribution by molecular

classes, with the proportion of radical and protonated ions (Figure 6-I). The second diagram is a box chart of the DBE median and percentile values by molecular classes (Figure 6-II).

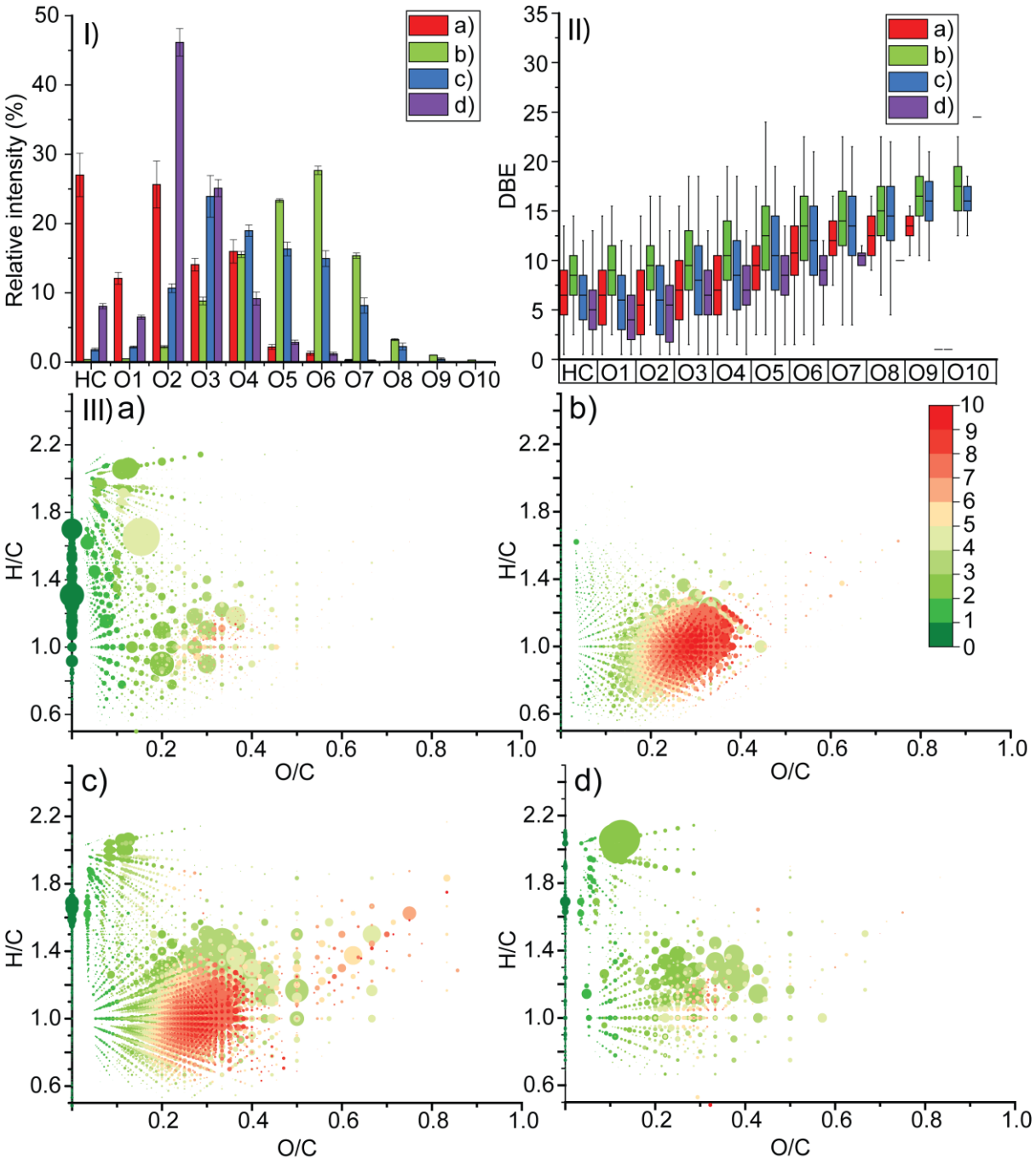

Figure 6. I) Relative intensity by molecular classes histogram, II) DBE 5th, 25th, 75th, 95th percentile, and median values by molecular classes box chart and III) Van Krevelen diagram of the four profile region extracted. a) Start of desorption, b) transition to advanced pyrolysis products, c) main pyrolysis products, and d) residues. For the relative intensity by molecular classes histogram, error bars were given at standard deviation of *n*=4. For the Van Krevelen diagram, colormap is characterized by number of oxygen atoms and the dot size, by relative intensity of ions.

At the start of the desorption profile (region a), the dominant molecular classes observed within Figure 6-I-a) were hydrocarbons and molecules with a number of oxygen atoms from one to four. The DBE

median value was around six and the 5th and 95th percentile value showed a high dispersion of DBE for the dominant classes (Figure 6-II-a). The Van Krevelen diagram (Figure 6-III-a) showed high abundance of hydrocarbons (O\C = 0). Other species with H/C value from 0.6 to 2.2 and low O/C values were found. This chemical specification was consistent with the commonly observed more volatile constituents described before, in GC-MS studies of wood extractible: coniferyl alcohol, sinapyl alcohol and other derivatives of monomeric lignin-degradation units.[40,41,42] Molecular formulae consistent with vanillin, syringaldehyde, eugenol, or fatty acids and fatty acid ester (high H/C value, low O/C value, and two oxygen atoms) were also found (Table S3).

In the region of maximum ion abundance (region b), compounds with four to seven oxygen atoms were observed in majority (Figure 6-I-b). The DBE median value was around thirteen. The 5th and 95th percentile values showed high dispersion of DBE for the dominant molecular classes, yet low dispersion for the other molecular classes. This median value was twice as high in this time region, compared to the start of the desorption profile (Figure 6-II-b). This information was linked to higher proportion of unsaturated molecules, such as lignin dimeric degradation products. The Van Krevelen diagram (Figure 6-III-b) displayed a molecular attribution area, with H/C ratios between 0.5 and 1.5, O/C between 0.1 and 0.5. This area contained attributions with one to ten oxygen atoms and was consistent with dimeric lignin degradation products, such as different combinations of the guaiacol (G) and syringyl (S) units (Table S3).[4]

When the signal from the pyrolysis profile started to decay (region c), the dominant molecular classes were molecules with oxygen atom number from two to seven. The median DBE values decreased for all molecular classes within this time region, compared to the region of maximum abundance (Figure 6-II-c). Besides, for this time region, the median DBE value for the hydrocarbons and median DBE value for molecules with one to four oxygen atoms were similar to the median DBE value from the beginning of the desorption profile. However, median DBE values for the molecules with five to ten oxygen atoms were lower during signal decay, compared to median DBE value from the maximum abundance region. Concerning the Van Krevelen diagram (Figure 6-III-c), two main molecular attribution area were found: one with H/C values between 0.5 and 1.5, O/C values between 0.1 and 0.5 containing various number of oxygen atoms, and a second one with H/C values between 1.5 and 2.4, O/C values between 0.1 and 0.2, containing few oxygen atoms. The first area was mostly made of lignin degradation products (monomeric and dimeric), and the second area was made of fatty acid like compounds.

Finally, the end of the desorption profile (region d) was dominated by compounds with two and three oxygen atoms (Figure 6-I-d). The median DBE value was the lowest of all the time region selected (Figure 6-II-d). The Van Krevelen diagram (Figure 6-III-d) had similarities with the Figure 6-III-a diagram corresponding to the start of the desorption profile, with diverse H/C values, low O/C values, and few oxygen atoms. Higher temperatures at the end of the pyrolysis should be associated nonetheless with less volatile species than during the beginning of the pyrolysis process. In fact, at the end of the pyrolysis process, lignin monomeric degradation products with fewer oxygen atoms were more intense compared to the dimeric degradation products.

As the Bruker DIP source is not well sealed, some amount of oxygen may be present and could react with the pyrolysis products to form oxygenated compounds. Previous experiments with polyethylene (PE) and polypropylene (PP) by DIP-APCI FTICR MS analysis[43], have shown compounds with insertion of oxygen atoms. However, with more polar molecules, such oxidation is generally not observed.[44] As lignocellulosic biomass contains a lot of oxygen, the increase in oxygen number in the attributed molecules in fractions (b) and (c), was more consistent with lignocellulosic degradation compounds rather than oxidation reactions.

Comparison of three wood species

Beech, oak, and maple wood pellet species were compared using DIP-APCI FTICR MS. Four analytical replicates were acquired for each wood type. The molecular formula attribution lists of the 12 data sets were merged into a list containing over 5,900 molecular formulae. Then, this list was subjected to multivariate data analysis. After analysis of variance (ANOVA) and extraction of significant features (p-values < 0.01), roughly 800 molecular formulae were subjected to PCA. Figure 7 illustrates the score plot for the first two principal components (PC1 and PC2), which explained nearly 85 % of the total variance. The PC1 score, which accounted for 76 % of the variance, was positive for beech pellets and negative for maple and oak. This PC1 score allowed a separation between beech and non-beech wood types.

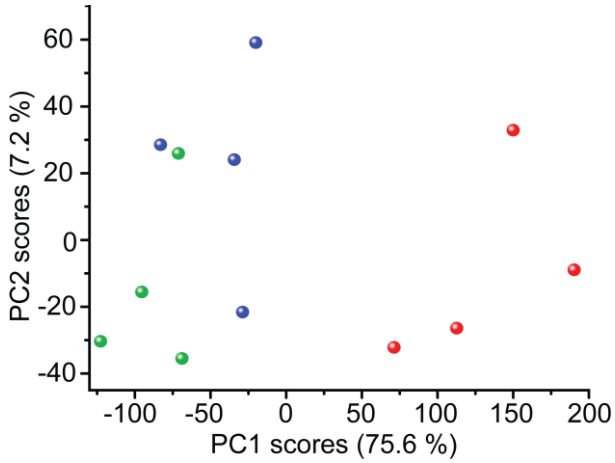

Figure 7. Score plot from PCA visualizing the first and second principal component (~ 85 % of total variance), with beech samples in red, maple in blue, and Oak in green

In Figure 8, a Van Krevelen plot, representing the 800 molecular formulae, was color-coded according to the values obtained for the PC1 loadings. The dot size represented the ion abundance observed for each molecular formula: Figure 8a represents the relative intensities from the mass spectra obtained from beech, and Figure 8b represents the relative intensities from the mass spectra obtained from oak and maple summed together.

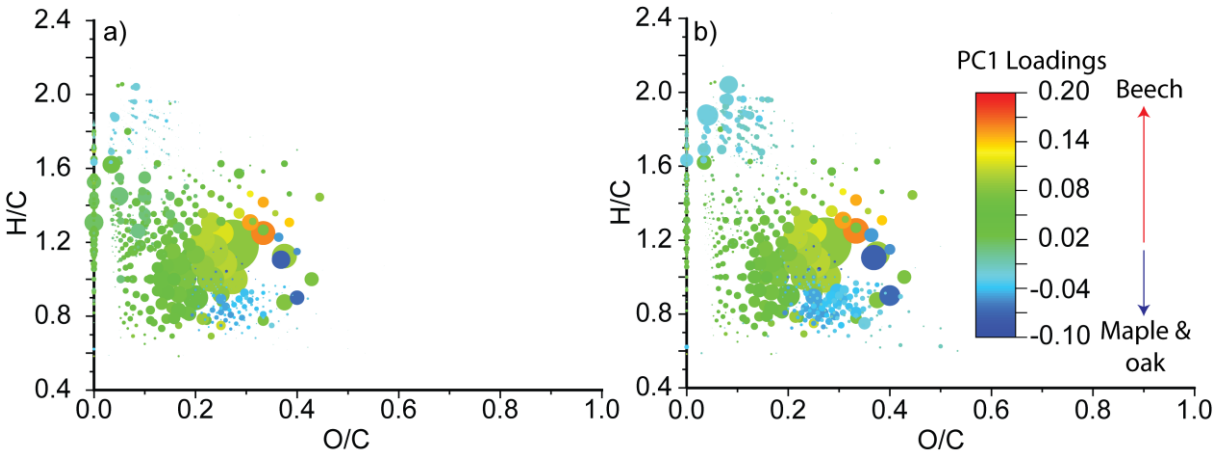

Figure 8. Modified Van-Krevelen plot color-coded with the loadings from PC1: a) for beech and b) for maple and oak. The size of dots was linked to relative intensity.

The molecular attributions with positive PC1 loadings (from 0.02 to 0.08: green color), which were expected to be characteristic constituents for beech pellets, were mostly found in the area of O/C ratio between 0.05 and 0.20, and H/C < 1.5. Such ratios were consistent with aromatic compounds with a low number of oxygen atoms, such as monomeric lignin degradation products. Conversely, molecular attributions with negative PC1 loadings (from 0 to -0.10: blue color), which should be more characteristic for oak and maple, were found in two areas. The first one, with O/C ratio between 0.2 and 0.4, and H/C < 1.3, corresponded to lignin dimeric degradation products. The second one, with O/C ratio between 0.05 and 0.2, and H/C > 1.5 were consistent with fatty acid-like compounds. The observation of relative intensities by molecular classes (Figure S8-a) showed for molecular formulae with positive PC1 loadings, the domination of molecular classes with one to three oxygen atoms. The molecules from these CHO_{1-3} classes, displayed median DBE values around 6 (Figure S8-b), which were consistent with monomeric lignin degradation products, and coherent with Figure 6 observations. Study of relative intensities by molecular classes (Figure S8-a) showed for molecular attribution with negative PC1 loadings, molecular classes containing seven to nine oxygen atoms. The molecules from these CHO_{7-9} classes displayed median DBE values around 17 (Figure S8-b), which were consistent with dimeric lignin degradation products. These results indicate the potential of DIP-APCI/APPI FTMS as a fingerprinting technique for the identification of pellet types on the molecular level. Outliers might be easily detected for this complex solid matrix, which is typically problematic to analyze with other methods.

Conclusion

In this study, an analytical method was developed for the characterization of solid lignocellulosic biomass samples, using DIP-APCI/APPI FTICR MS. The DIP method developed here allowed fast analysis of ground wood pellets, using two different ionization techniques. With its high resolving power, the FTICR mass analyzer provided the attribution of molecular formulae, including information on isobaric compounds. The molecular attribution lists were used in graphical representations, which give information on the chemical space of ground wood pellets thermal degradation products. The comparison of the two ionization sources showed that APCI was generic to oxygenated lignocellulosic biomass degradation compounds, such as fatty acids, lignin, and sugars. The APPI source, in the absence of any dopant, was specific to polyphenolic and lignin compounds. The DIP method permitted to monitor the ions obtained during the thermo-desorption and pyrolysis process, which can be interesting to observe the degradation mechanism of lignocellulosic biomass. The comparison of the DIP data obtained from three wood species (oak, maple, and beech) using PCA showed significant differences of chemical space between beech and oak/maple samples. This DIP-APCI/APPI FTICR MS method could be used to differentiate other lignocellulosic biomass samples and to find molecular fingerprints for different wood species with a more thorough study of the specific molecular attributions of each wood types. The DIP-APCI/APPI FTICR MS that we had developed allowed the characterization of lignocellulosic biomass and is a useful tool to compare wood samples.

Electronic supplementary information

Supplementary data includes information on DIP setup and parameters, scan-to-scan recalibration, Venn diagram from molecular attribution, putative structure of wood degradation products and plots linked to PC loadings.

Acknowledgements

The COBRA laboratory is financed by the Labex SynOrg (ANR-11-LABX-0029) and the European Regional Development Fund (ERDF HN0001343).

References

1. Kan, T.; Strezov, V.; Evans, T. J., Lignocellulosic biomass pyrolysis: A review of product properties and effects of pyrolysis parameters. *Renew. Sust. Energ. Rev.* **2016,** *57*, 1126-1140.
2. Pöschl, U., Atmospheric Aerosols: Composition, Transformation, Climate and Health Effects. *Angew. Chem. Int. Ed.* **2005,** *44* (46), 7520-7540.
3. Laumbach, R. J.; Kipen, H. M., Respiratory health effects of air pollution: Update on biomass smoke and traffic pollution. *J. Allergy Clin. Immunol.* **2012,** *129* (1), 3-11.
4. Adler, E., Lignin chemistry—past, present and future. *Wood. Sci. Technol.* **1977,** *11* (3), 169-218.
5. Martinez, A. T.; Speranza, M.; Ruiz-Duenas, F. J.; Ferreira, P.; Camarero, S.; Guillen, F.; Martinez, M. J.; Gutierrez, A.; del Rio, J. C., Biodegradation of lignocellulosics: microbial, chemical, and enzymatic aspects of the fungal attack of lignin. *Int Microbiol* **2005,** *8* (3), 195-204.
6. Kirk, T. K.; Farrell, R. L., Enzymatic "Combustion": The Microbial Degradation of Lignin. *Annu. Rev. Microbiol.* **1987,** *41* (1), 465-501.
7. Yang, H.; Yan, R.; Chen, H.; Lee, D. H.; Zheng, C., Characteristics of hemicellulose, cellulose and lignin pyrolysis. *Fuel* **2007,** *86* (12), 1781-1788.
8. Coats, A. W.; Redfern, J. P., Thermogravimetric analysis. A review. *Analyst* **1963,** *88* (1053), 906-924.
9. Holdiness, M. R., Evolved gas analysis by mass spectrometry: A review. *Thermochim. Acta* **1984,** *75* (3), 361-399.
10. Materazzi, S.; Risoluti, R., Evolved Gas Analysis by Mass Spectrometry. *Appl. Spectrosc. Rev.* **2014,** *49* (8), 635-665.
11. Guzzonato, A.; Mehlmann, H.; Krumwiede, D.; Harrad, S., A novel method for quantification of decabromodiphenyl ether in plastics without sample preparation using direct insertion probe – magnetic sector high resolution mass spectrometry. *Anal. Methods* **2016,** *8* (27), 5487-5494.
12. Flego, C.; Zannoni, C., Direct Insertion Probe–Mass Spectrometry (DIP–MS) Maps and Multivariate Analysis in the Characterization of Crude Oils. *Energy. Fuels.* **2012,** *27* (1), 46-55.
13. Flego, C.; Carati, C.; Gaudio, L. D.; Zannoni, C., Direct Mass Spectrometry of tar sands: A new approach to bitumen identification. *Fuel* **2013,** *111*, 357-366.
14. Flego, C.; Zannoni, C., Direct Insertion Probe−Mass Spectrometry: A Useful Tool for Characterization of Asphaltenes. *Energy. Fuels.* **2010,** *24* (11), 6041-6053.
15. Christensen, E.; Evans, R. J.; Carpenter, D., High-resolution mass spectrometric analysis of biomass pyrolysis vapors. *J. Anal. Appl. Pyrolysis* **2017,** *124*, 327-334.
16. McEwen, C. N.; McKay, R. G.; Larsen, B. S., Analysis of Solids, Liquids, and Biological Tissues Using Solids Probe Introduction at Atmospheric Pressure on Commercial LC/MS Instruments. *Anal. chem.* **2005,** *77* (23), 7826-7831.
17. Farenc, M.; Corilo, Y. E.; Lalli, P. M.; Riches, E.; Rodgers, R. P.; Afonso, C.; Giusti, P., Comparison of Atmospheric Pressure Ionization for the Analysis of Heavy Petroleum Fractions with Ion Mobility-Mass Spectrometry. *Energy. Fuels.* **2016,** *30* (11), 8896-8903.
18. Barrère, C.; Maire, F.; Afonso, C.; Giusti, P., Atmospheric Solid Analysis Probe–Ion Mobility Mass Spectrometry of Polypropylene. *Anal. chem.* **2012,** *84* (21), 9349-9354.
19. Bruns, E. A.; Perraud, V.; Greaves, J.; Finlayson-Pitts, B. J., Atmospheric Solids Analysis Probe Mass Spectrometry: A New Approach for Airborne Particle Analysis. *Anal. chem.* **2010,** *82* (14), 5922-5927.
20. Marshall, A. G.; Rodgers, R. P., Petroleomics: Chemistry of the underworld. *Proc. Natl. Acad. Sci. U.S.A.* **2008,** *105* (47), 18090.

21. Purcell, J. M.; Juyal, P.; Kim, D.-G.; Rodgers, R. P.; Hendrickson, C. L.; Marshall, A. G., Sulfur Speciation in Petroleum: Atmospheric Pressure Photoionization or Chemical Derivatization and Electrospray Ionization Fourier Transform Ion Cyclotron Resonance Mass Spectrometry. *Energy. Fuels.* **2007,** *21* (5), 2869-2874.
22. Ruger, C. P.; Sklorz, M.; Schwemer, T.; Zimmermann, R., Characterisation of ship diesel primary particulate matter at the molecular level by means of ultra-high-resolution mass spectrometry coupled to laser desorption ionisation--comparison of feed fuel, filter extracts and direct particle measurements. *Anal Bioanal Chem* **2015,** *407* (20), 5923-37.
23. Wei, J.; Bristow, A.; McBride, E.; Kilgour, D.; O'Connor, P. B., D-alpha-tocopheryl polyethylene glycol 1000 succinate: a view from FTICR MS and tandem MS. *Anal Chem* **2014,** *86* (3), 1567-74.
24. Pouwels, A. D.; Boon, J. J., Analysis of beech wood samples, its milled wood lignin and polysaccharide fractions by curie-point and platinum filament pyrolysis-mass spectrometry. *J. Anal. Appl. Pyrolysis* **1990,** *17* (2), 97-126.
25. Ingemarsson, Å.; Nilsson, U.; Nilsson, M.; Pedersen, J. R.; Olsson, J. O., Slow pyrolysis of spruce and pine samples studied with GC/MS and GC/FTIR/FID. *Chemosphere* **1998,** *36* (14), 2879-2889.
26. Ruger, C. P.; Miersch, T.; Schwemer, T.; Sklorz, M.; Zimmermann, R., Hyphenation of Thermal Analysis to Ultrahigh-Resolution Mass Spectrometry (Fourier Transform Ion Cyclotron Resonance Mass Spectrometry) Using Atmospheric Pressure Chemical Ionization For Studying Composition and Thermal Degradation of Complex Materials. *Anal Chem* **2015,** *87* (13), 6493-9.
27. Rogge, W. F.; Hildemann, L. M.; Mazurek, M. A.; Cass, G. R., Sources of Fine Organic Aerosol. 9. Pine, Oak, and Synthetic Log Combustion in Residential Fireplaces. *Environ. Sci. Technol.* **1998,** *32* (1), 13-22.
28. Robb, D. B.; Covey, T. R.; Bruins, A. P., Atmospheric Pressure Photoionization: An Ionization Method for Liquid Chromatography−Mass Spectrometry. *Anal. chem.* **2000,** *72* (15), 3653-3659.
29. Heberle, H.; Meirelles, G. V.; da Silva, F. R.; Telles, G. P.; Minghim, R., InteractiVenn: a web-based tool for the analysis of sets through Venn diagrams. *BMC. Bioinformatics.* **2015,** *16* (1), 169.
30. Kekäläinen, T.; Venäläinen, T.; Jänis, J., Characterization of Birch Wood Pyrolysis Oils by Ultrahigh-Resolution Fourier Transform Ion Cyclotron Resonance Mass Spectrometry: Insights into Thermochemical Conversion. *Energy. Fuels.* **2014,** *28* (7), 4596-4602.
31. Smith, E. A.; Park, S.; Klein, A. T.; Lee, Y. J., Bio-oil Analysis Using Negative Electrospray Ionization: Comparative Study of High-Resolution Mass Spectrometers and Phenolic versus Sugaric Components. *Energy. Fuels.* **2012,** *26* (6), 3796-3802.
32. Syage, J. A., Mechanism of [M + H]+ formation in photoionization mass spectrometry. *J. Am. Soc. Mass Spectrom.* **2004,** *15* (11), 1521-1533.
33. Horning, E. C.; Horning, M. G.; Carroll, D. I.; Dzidic, I.; Stillwell, R. N., New picogram detection system based on a mass spectrometer with an external ionization source at atmospheric pressure. *Anal. chem.* **1973,** *45* (6), 936-943.
34. Vaikkinen, A.; Kauppila, T. J.; Kostiainen, R., Charge Exchange Reaction in Dopant-Assisted Atmospheric Pressure Chemical Ionization and Atmospheric Pressure Photoionization. *J. Am. Soc. Mass Spectrom.* **2016,** *27* (8), 1291-1300.
35. Kim, S.; Kramer, R. W.; Hatcher, P. G., Graphical Method for Analysis of Ultrahigh-Resolution Broadband Mass Spectra of Natural Organic Matter, the Van Krevelen Diagram. *Anal. chem.* **2003,** *75* (20), 5336-5344.
36. Podgorski, D. C.; Hamdan, R.; McKenna, A. M.; Nyadong, L.; Rodgers, R. P.; Marshall, A. G.; Cooper, W. T., Characterization of Pyrogenic Black Carbon by Desorption Atmospheric Pressure Photoionization Fourier Transform Ion Cyclotron Resonance Mass Spectrometry. *Anal. chem.* **2012,** *84* (3), 1281-1287.
37. Shen, D. K.; Gu, S., The mechanism for thermal decomposition of cellulose and its main products. *Bioresourc. Technol.* **2009,** *100* (24), 6496-6504.

38. White, R. H.; Dietenberger, M. A., Wood Products: Thermal Degradation and Fire. In *Encyclopedia of Materials: Science and Technology*, Buschow, K. H. J.; Cahn, R. W.; Flemings, M. C.; Ilschner, B.; Kramer, E. J.; Mahajan, S.; Veyssière, P., Eds. Elsevier: Oxford, 2001; pp 9712-9716.
39. Harrison, A. G., *Chemical Ionization Mass Spectrometry, Second Edition*. Taylor & Francis: 1992.
40. Vichi, S.; Santini, C.; Natali, N.; Riponi, C.; López-Tamames, E.; Buxaderas, S., Volatile and semi-volatile components of oak wood chips analysed by Accelerated Solvent Extraction (ASE) coupled to gas chromatography–mass spectrometry (GC–MS). *Food. Chem.* **2007,** *102* (4), 1260-1269.
41. Pérez-Coello, M. S.; Sanz, J.; Cabezudo, M. D., Analysis of volatile components of oak wood by solvent extraction and direct thermal desorption-gas chromatography-mass spectrometry. *J. Chrom. A* **1997,** *778* (1), 427-434.
42. Pérez-Coello, M. S.; Sanz, J.; Cabezudo, M. D., Determination of Volatile Compounds in Hydroalcoholic Extracts of French and American Oak Wood. *Am. J. Enol. Viticult. 1***999,** *50* (2), 162.
43. Farenc, M.; Witt, M.; Craven, K.; Barrère-Mangote, C.; Afonso, C.; Giusti, P., Characterization of Polyolefin Pyrolysis Species Produced Under Ambient Conditions by Fourier Transform Ion Cyclotron Resonance Mass Spectrometry and Ion Mobility-Mass Spectrometry. *J. Am. Soc. Mass Spectrom.* **2017,** *28* (3), 507-514.
44. Cossoul, E.; Hubert-Roux, M.; Sebban, M.; Churlaud, F.; Oulyadi, H.; Afonso, C., Evaluation of atmospheric solid analysis probe ionization coupled to ion mobility mass spectrometry for characterization of poly(ether ether ketone) polymers. *Anal. Chim. Acta* **2015,** *856*, 46-53.

For Table of Contents Only